



Near-fault strong motion complexity of the 2000 Tottori earthquake (Japan) from a broadband source asperity model

N. Pulido^{a,*}, T. Kubo^{a,b}

^a*Earthquake Disaster Mitigation Research Center; EDM, NIED,*

4F Human Renovation Museum, 1-5-2, Kaigan-dori, Wakahama, Chuo-ku, Kobe 651-0073, Japan

^b*Earthquake Disaster Mitigation Research Center, NIED/School of Engineering, The University of Tokyo, Bunkyo-ku, Tokyo 113-8656, Japan*

Received 16 January 2002; received in revised form 23 September 2002; accepted 9 March 2004

Available online 18 September 2004

Abstract

The October 6/2000 Tottori earthquake that occurred in central Japan was an intermediate size strike-slip event that produced a very large number of near field strong motion recordings. The large amount of recorded data provides a unique opportunity for investigating a source asperity model of the Tottori earthquake that, combined with a hybrid strong motion simulation technique, is able to reproduce the observed broadband frequency near-fault ground motion.

We investigated the optimum source asperity parameters of the Tottori earthquake, by applying a Genetic Algorithm (GA) inversion scheme to optimise the fitting between simulated and observed response spectra and Peak Ground Acceleration (PGA) values. We constrained the initial model of our inversion by using the heterogeneous slip distribution obtained from a kinematic inversion of the source of previous studies. We used all the observed near-fault ground motions (–100 m) from the borehole strong motion network of Japan (KiK-Net), which are little affected by surficial geology (site effects).

The calculation of broadband frequency strong ground motion (0.1–10 Hz) is achieved by applying a hybrid technique that combines a deterministic simulation of the wave propagation for the low frequencies and a semi-stochastic modelling approach for the high frequencies. For the simulation of the high frequencies, we introduce a frequency-dependent radiation pattern model that efficiently removes the dependence of the pattern coefficient on the azimuth and take-off angle as the frequency increases. The good agreement between the observed and simulated broadband ground motions shows that our inversion procedure is successful in estimating the optimum asperity parameters of the Tottori earthquake and provides a good test for the strong ground motion simulation technique.

The ratio of background stress drop to average asperity stress drop from our inversion is nearly 50%, in agreement with the theoretical asperity model of Das and Kostrov [Das, S., Kostrov, B.V., 1986. Fracture of a single asperity on a finite fault: a model for weak earthquakes? *Earthquake Source Mechanics*, AGU, pp. 91–96.], and an empirical ratio of asperities to rupture area [Seismol. Res. Lett. 70 (1999) 59–80.].

The simulated radiation pattern is very complex for epicentral distances within half the fault length, but it approaches the radiation of a double-couple point source for larger distances.

* Corresponding author. Tel.: +81 794 83 6637; fax: +81 794 83 6695.

E-mail address: nelson@edm.bosai.go.jp (N. Pulido).

The rupture velocity and rise time have a significant influence on the Peak Ground Velocity (PGV) distribution around the fault. An increase in rupture velocity produces a similar effect on the ground motion as a reduction in rise time.

© 2004 Elsevier B.V. All rights reserved.

Keywords: Strong motion simulation; Source asperity model; Non-linear inversion; 2000 Western Tottori Prefecture earthquake

1. Introduction

The 2000 Western Tottori Prefecture earthquake ($M_w=6.8$) is the largest earthquake to hit Japan since the 1995 Hyogo-ken Nanbu (Kobe) earthquake. The Tottori earthquake produced a very large amount of near field strong ground motion recordings from the K-Net and KiK-Net, which were deployed after 1995. In particular, the KiK-Net, which is a nationwide network of 500 instrumented boreholes with an average depth of 100 m, is very useful for studying the contribution from the source to the subsequent ground motion.

The simulation of near field ground motion represents a very difficult problem since it is affected by the complexity of source and site effects. Kinematic models have been widely developed in order to account for heterogeneous source characteristics and underground geology. These models are very efficient in explaining source directivity effects as well as effects of underground geology on ground motion (Pitarka et al., 1998). However, the ground motion simulation from those models is only practical for frequencies below 1 Hz.

Recently, hybrid ground motion techniques have been proposed to obtain broadband frequency near-fault ground motions by combining deterministic modelling for the low frequencies and the stochastic approach for high frequencies. The hybrid ground motion simulation technique, first proposed by Kamae et al. (1990, 1998), combined a deterministic modelling of the low frequencies with the high-frequency stochastic approach of Boore (1983), and the summation technique of Irikura (1986). These models were successful in explaining the general characteristics of ground motion near the fault during the Hyogo-ken Nanbu earthquake (Kamae et al., 1998; Pitarka et al., 2000). However, their representation of the radiation pattern at high frequencies is not completely isotropic (Pulido, 2002).

Our methodology is an improvement of Kamae et al. (1990, 1998) and Pitarka et al. (2000). In this

paper, we introduce a frequency-dependent radiation pattern model for the simulation of high frequencies, which efficiently removes the dependence of the radiation pattern coefficient on the source–receiver azimuth and take-off angle as the frequency increases. Our model applies a smooth transition between the theoretical non-spherical radiation at low frequencies (double couple) to a complete spherical (isotropic) radiation at high frequencies.

We performed a systematic search for the optimum asperity and high-frequency attenuation parameters (asperity and background stress drops and $Q(f)$), by applying a non-linear inversion scheme to optimise the fitting between observed and simulated broadband frequency ground motions.

2. Ground motion estimation methodology

We estimate the broadband frequency (0.1–10 Hz) near-fault ground motion from a hybrid simulation technique that combines deterministic wave propagation modelling for the low frequencies with a stochastic technique for the high frequencies. The basic idea of the simulation methodology is to evaluate the strong ground motion radiated from a finite fault source model composed of asperities embedded in a flat layered velocity structure. The ground motion at a particular site is obtained from the contributions of the seismic radiation from all the asperities in the fault plane that are assumed to have a finite area.

2.1. Low-frequency ground motion

To calculate low-frequency ground motion (0.1–1.0 Hz), we subdivide the asperity into several subfaults or point sources and simply add the time delayed ground motion from them by applying a constant rupture velocity. The seismogram from each point source is obtained numerically by the Discrete Wave Number method of Bouchon (1981), which computes the wave

propagation in a flat-layered crustal velocity structure, for a particular focal mechanism and source moment function. The point source moment function is defined as a smoothed ramp as follows:

$$M(t) = \frac{M_0}{2} * \left(1 + \tanh\left(\frac{4*(t - \tau/2)}{\tau}\right) \right) \quad (1)$$

where M_0 is the point source seismic moment, t is the rupture time, and τ is the asperity rise time.

2.2. High-frequency ground motion

High-frequency ground motion (1–10 Hz) is calculated from a finite asperity as before, but the point source ground motions are obtained from the stochastic approach of Boore (1983). The procedure of summation of the point source contributions differ from the one applied for the low frequencies; for high frequencies, the summation is obtained by applying the empirical Green's function method proposed by Irikura (1986), which is very efficient for the radiation of high-frequency ground motion from finite faults.

We introduce a frequency-dependent radiation pattern $R_{pi}(\theta, \phi, f)$ in order to account for the effect of the pattern on intermediate frequency ground motions (1–3 Hz). The i component of acceleration Fourier spectra for a point source is obtained as follows:

$$A_i(f) = \frac{R_{pi}(\theta, \phi, f) M_0 S(f, f_c) F_s e^{-\pi f R/Q(f) \beta} P(f, f_{\max})}{4\pi\rho\beta^3 R} \quad (2)$$

$$f_c = 49000\beta(\Delta\sigma/M_0)^{1/3} \quad (3)$$

$$P(f, f_{\max}) = \frac{1}{\sqrt{(1 + f/f_{\max})}} \quad (4)$$

where M_0 is the point source seismic moment (in N m; Eq. (3)), $S(f, f_c)$ is the omega square source model (Brune, 1970) with corner frequency f_c (Eq. (3)), $\Delta\sigma$ is the point source stress drop (in MPa), F_s is the amplification factor due to the free surface, R is the station-point source distance and ρ and β are the average density and S-wave velocity of the media. The exponential term accounts for the regional attenuation of Q which increases with the frequency as a power law of the form af^b , where a and b determine the strength of

attenuation. P is the high-frequency cut-off of the point-source acceleration spectra for frequencies above f_{\max} (Eq. (4)).

2.3. High-frequency radiation pattern

It has been traditionally assumed that the radiation pattern at high frequencies does not follow the theoretical radiation pattern of a double couple. However, analysis from various near-fault recordings have shown that the radiation pattern at the intermediate frequency range (1–4 Hz) is not purely stochastic but is characterized by a transition from the theoretical double-couple radiation pattern at low frequencies to a completely stochastic isotropic radiation pattern at high frequencies (Liu and Helmberger, 1985; Akazawa et al., 2000; Satoh, 2002a,b; Takenaka et al., 2003). From an analysis of the aftershocks of the March 26 and May 13, 1997 Kagoshima earthquake sequence $M_{JMA}=6.5$ and $M_{JMA}=6.3$ (Japan), it has been observed that the energy contribution from the SH and SV waves to the total S-wave radiation is almost equal at high frequencies (Takenaka, 2003). A similar result was found by Satoh (2002a) from an analysis of aftershocks of an earthquake in Northern Japan ($M_w=5.0$).

Considering the previous observations, we elaborated a radiation pattern model that makes a smooth transition between the theoretical double-couple radiation for frequencies lower than 1 Hz to an isotropic spherical radiation for frequencies larger than 3 Hz. The radiation pattern coefficient R_{pi} at a particular receiver for the i component of ground motion, is obtained as follows:

$$R_{pi}(\theta, \phi, f) = F_i(\phi_s, \delta, \lambda, \theta, \phi) \quad \text{for } f \leq f_1$$

$$R_{pi}(\theta, \phi, f) = F_i(\phi_s, \delta, \lambda, \theta, \phi) + \frac{(f - f_1)}{(f_2 - f_1)} \times \left(\frac{1}{\sqrt{2}} R_{S,ave} - F_i(\phi_s, \delta, \lambda, \theta, \phi) \right) \quad \text{for } f_1 < f < f_2$$

$$R_{pi}(\theta, \phi, f) = \frac{1}{\sqrt{2}} R_{S,ave} \quad \text{for } f \geq f_2 \quad (5)$$

where $F_i(\phi_s, \delta, \lambda, \theta, \phi)$ is the i component (ns, ew or ud) of the theoretical radiation pattern coefficient of a double couple with strike ϕ_s , dip δ and rake λ , at receiver with take-off angle θ and azimuth ϕ (Aki and Richards, 2002, Eqs. 4.88, 4.90 and 4.91). We only consider contributions from the SH and SV radiation pattern coefficients. The basic idea in Eq. (5) is to apply a smooth transition from F_i to an average radiation pattern coefficient ($R_{S,ave}$) as the frequency

increase. We assume a linear variation of R_{pi} from a frequency f_1 to a frequency f_2 , with $f_1=1$ Hz and $f_2=3$ Hz.

$R_{S,ave}$ is the average radiation pattern coefficient for the total S-wave, calculated for all rays departing in the upper focal sphere (θ from 90° to 180°) which corresponds to the near-fault region, and divided by $\sqrt{2}$ to account for the S-wave partition in two components. $R_{S,ave}$ is cal-

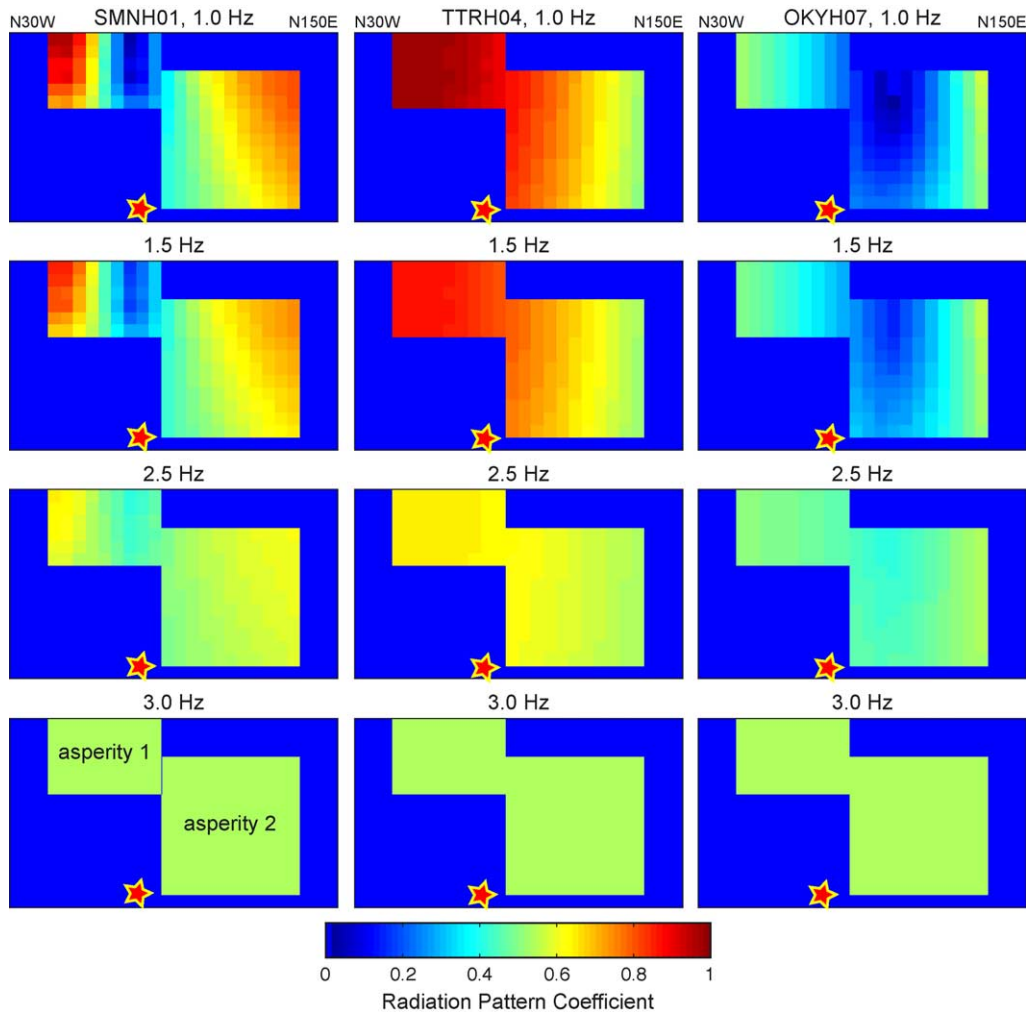


Fig. 1. Radiation pattern coefficient distribution across the fault plane (only asperities) at SMNH01, TTRH07 and OKYH07 stations, for frequencies of 1.0, 1.5, 2.5 and 3.0 Hz. We can observe the regions located at a nodal plane and maximum radiation plane of S-waves, for frequencies near 1.0 Hz. The azimuth and take-off angle dependence of the radiation pattern coefficient is efficiently removed as the frequency increases to 3 Hz.

culated by using the approach of Boore and Boatwright (1984) as follows:

$$R_{S,ave} = \left[\sum_{i=SH,SV} \left(\frac{\int_{\pi/2}^{\pi} \int_0^{2\pi} F_i(\phi_s, \lambda, \delta, \theta, \phi) \sin\theta d\phi d\theta}{\int_{\pi/2}^{\pi} \int_0^{2\pi} \sin\theta d\phi d\theta} \right)^2 \right]^{1/2} \quad (6)$$

See Eq. (5) for parameter definitions. From Eq. (6), we obtained a $R_{S,ave}$ value of 0.55 for a vertical, strike-slip fault.

2.4. Radiation pattern coefficient of asperities

We calculated the radiation pattern coefficient for every point source within asperities (Eq. (5)), at all the simulation points (Fig. 4). We used the crustal velocity model of the Tottori region (DPRI, 2000) to estimate the take-off angle of the direct S-wave, at every source–station raypath. In Fig. 1, we show the radiation pattern coefficient distribution across the fault plane (asperities only) at SMNH01, TTRH04 and OKYH07 stations, for 1.0, 1.5, 2.5 and 3 Hz. The S-wave radiation pattern coefficient has a large variability across the fault plane near 1 Hz (Fig. 1). We can observe the regions in the fault plane that correspond to an S-wave nodal plane, when the pattern coefficient approaches 0 (SMNH01 and OKYH07 stations), as well as regions corresponding to a plane of maximum S-wave radiation, when the coefficient approaches 1 (SMNH01 and TTRH04 stations). Our model efficiently removes the dependence of the radiation pattern coefficient on the azimuth and take-off angle (or subfault depth) as the frequency increases (Fig. 1). For frequencies larger than 3 Hz, the radiation of S-waves is completely isotropic, in agreement with analyses of earthquake data (Takenaka, 2003; Satoh, 2002a,b).

For the simulation of high-frequency ground motion at a given receiver, we calculated an average asperity radiation pattern coefficient for all point

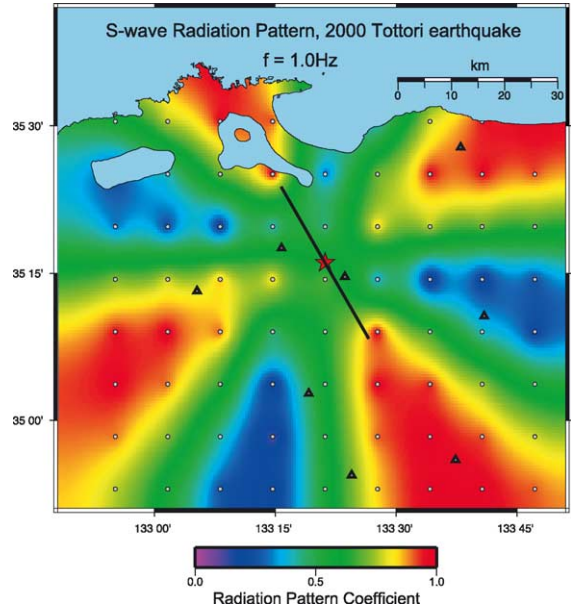


Fig. 2. Simulated S-wave radiation pattern from asperity 1 at 1.0 Hz. For distances within half a fault length, the pattern has a uniform value of 0.55. For larger distances, the pattern approaches the radiation of a double couple.

source–receiver raypaths within the asperity, at every frequency. Then we calculated the ground motion by using a site, asperity and frequency-specific radiation pattern coefficient (Eq. (2)). In Fig. 2, we show the spatial distribution of the average radiation pattern coefficient of asperity 1 (complete S-wave) at 1 Hz. For distances within half a fault length from the epicentre, the radiation pattern has a uniform value of 0.55. However, for larger distances, the pattern approaches the radiation of a double-couple point source (Fig. 2). The pattern distribution is completely uniform at 3 Hz.

3. Velocity structure Tottori region

For the calculation of the low-frequency ground motion, we use a flat-layered velocity structure obtained by overlapping the crustal velocity model of the Tottori region (DPRI, 2000) with the KiK-Net borehole information. The crustal model was slightly modified at every station (except SMNH02 and OKYH09) to improve the agreement of the waveforms for periods larger than 5 s (Fig. 3).

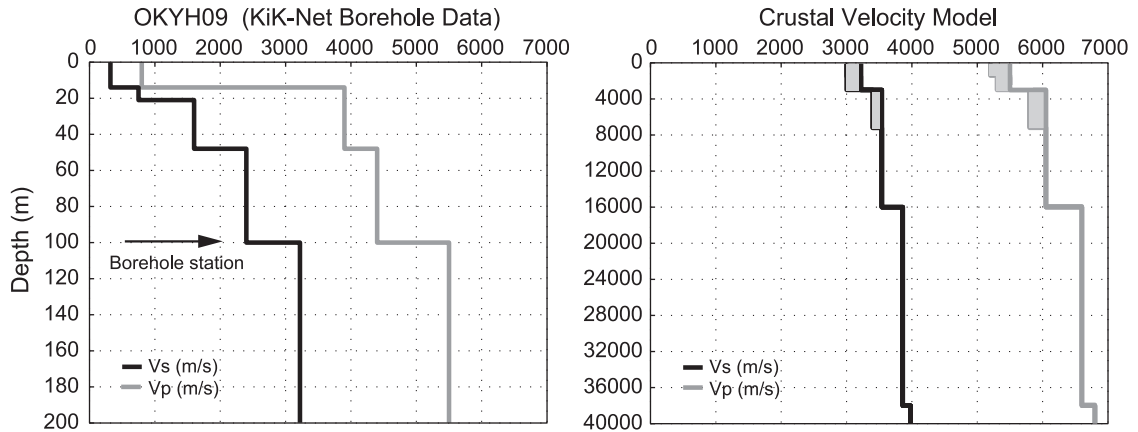


Fig. 3. (a) Shallow velocity structure at OKYH09 station obtained from the KiK-Net borehole database. (b) Crustal velocity model of the Tottori region (DPRI, 2000). The crustal model was slightly modified at every station (except SMNH02 and OKYH09) for Vs and Vp values within the gray area.

We simulated the ground motion at all the KiK-Net borehole stations in near-fault region (Fig. 4). We used the waveforms recorded at the bottom

of the borehole, at an average depth of 100 m. In this way, we avoided shallow site effects and could concentrate on studying the contribution

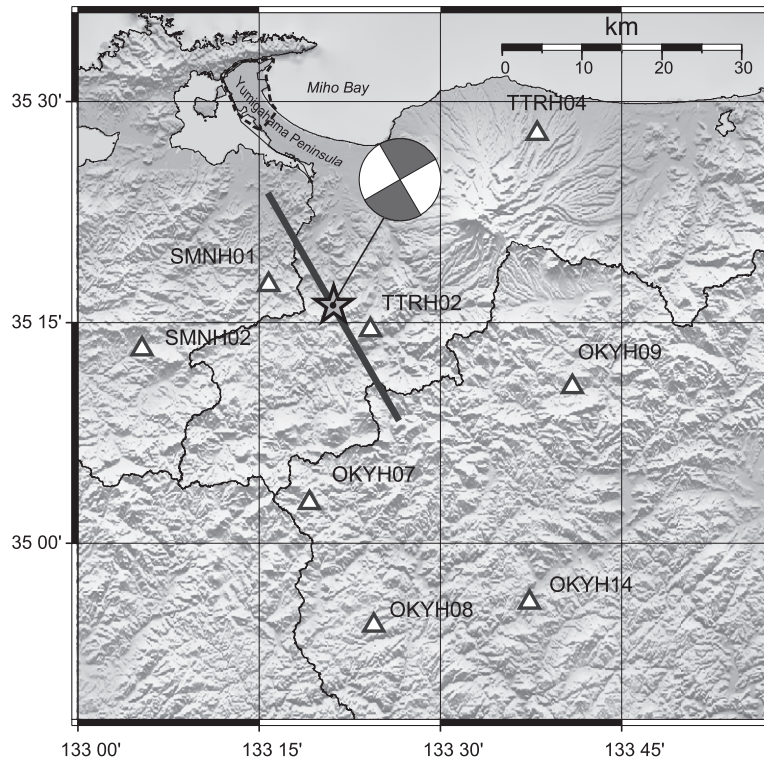


Fig. 4. Near-fault strong motion stations used for the hybrid ground motion simulation (shown by triangles). The accelerometers are located at an average depth of 100m. The 2000 Tottori earthquake was a left-lateral strike-slip earthquake ($M_w=6.8$). The fault mechanism is shown (strike 150° , dip 90° , slip 0°). The assumed fault plane is shown by a thick line.

of the heterogeneous source to the recorded ground motion.

4. Asperities and attenuation parameters

We estimated the asperity and attenuation parameters by optimizing the agreement between observed and simulated low-frequency waveforms and broadband frequency spectra, as shown in Fig. 5. We defined an initial asperity model by using the heterogeneous slip distribution of the Tottori earthquake obtained by a kinematic inversion of the source of previous studies (Iwata et al., 2000). Asperities were defined as regions in the fault plane enclosing an average slip 50% larger than the total fault average slip (Somerville et al., 1999). We estimated the area, location and seismic moment of asperities from the slip model of Iwata et al. (2000) (Table 1). The TTRH02 station was not used for the estimation of the

Table 1

Asperity parameters of the 2000 Tottori earthquake, unchanged for all the ground motion simulations

Asperity	Area (km ²)	Mo (N m)	f_{\max} (Hz)	Number of subfaults
1	9×6	3.1e18	6.1	24
2	10.5×10.5	7.2e18	6.1	36
Background	33×21	9.0e18	6.1	77

asperity parameters, but we calculated the broadband ground motion to pick up the corresponding Peak Ground Acceleration (PGA) and Peak Ground Velocity (PGV) values. Our asperity model consists of two large asperities located above the hypocenter, embedded in a background slip that corresponds to the entire fault rupture area (Fig. 6). The point sources within asperities and background region have the following focal mechanism: strike 150°, dip 90° and rake 0°.

We estimated the rise time and rupture velocity of asperities and background region by a trial-and-error procedure, to optimize the fitting in the low-frequency waveforms at the near-fault KiK-Net underground stations.

4.1. High-frequency parameters

The high-frequency content of the simulated ground motions is mainly controlled by three factors: the asperity and background stress drops, $Q(f)=af^b$ and f_{\max} . In order to investigate the optimum values

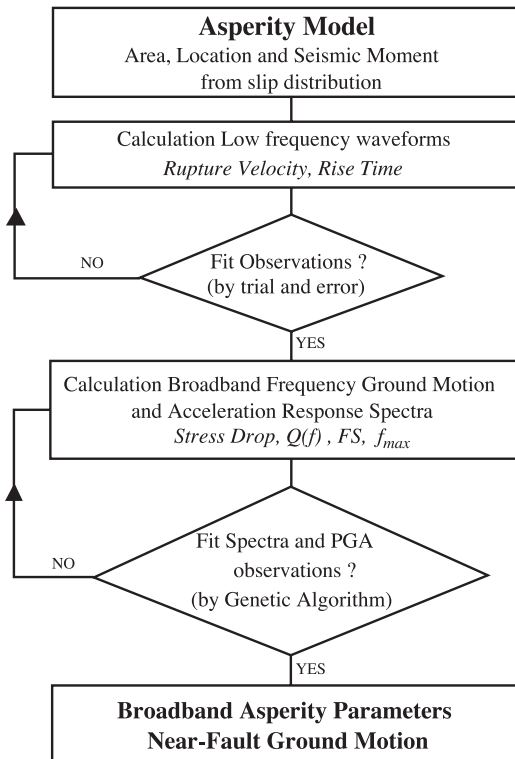


Fig. 5. Flow chart diagram of the asperities and attenuation parameters estimation procedure.

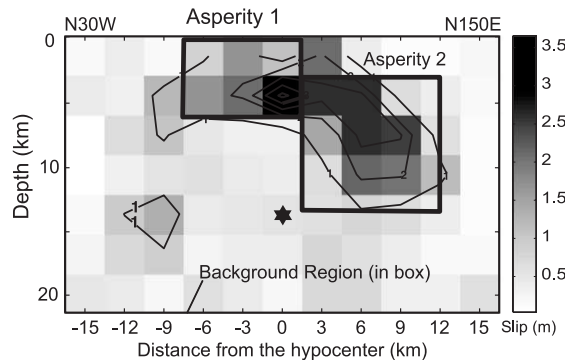


Fig. 6. Asperity model of the 2000 Western Tottori Prefecture earthquake. The model consists of two asperities and a background region as shown by the black rectangles. The heterogeneous slip distribution from a kinematic inversion of the source is shown in a gray scale (Iwata et al., 2000).

for these parameters, we inverted the observed acceleration response spectra at all KiK-Net near-fault stations (horizontal components). We applied a Genetic Algorithm (GA) inversion scheme (Houck et al., 1995) in order to maximize the fitting between the simulated and observed spectra. We used the rupture velocity and rise time values obtained previously. We decided to constraint f_{\max} in order to eliminate the trade-off with $Q(f)$. We used an f_{\max} value of 6.1 Hz, obtained from analyses of near-fault ground motion spectra of the Tottori earthquake (Sato, 2002b). We included the free surface coefficient (F_s) as a model parameter, in order to investigate the effect of downgoing S-waves to the borehole ground motion. The model parameters of our inversion are the following: $\Delta\sigma_{1,2,3}$ (stress drop asperity 1, asperity 2 and background region, respectively), F_s , a and b . We used the acceleration response spectra and the PGA values at every horizontal component to evaluate the fitness of the inversion:

$$fit_{\text{spectra}} = \frac{1}{2n} \sum_{i=1,n} \left[1 - \frac{\int (\text{Sa}_{\text{obs}} - \text{Sa}_{\text{sim}})^2 dT}{\int \text{Sa}_{\text{obs}}^2 dT} \right] \quad (7)$$

$$fit_{\text{PGA}} = \frac{1}{2n} \sum_{i=1,n} \left[1 - \frac{|\text{PGA}_{\text{obs}} - \text{PGA}_{\text{sim}}|}{|\text{PGA}_{\text{obs}}|} \right] \quad (8)$$

where n is the total number of stations, and Sa_{obs} and Sa_{sim} are the observed and simulated acceleration response spectra evaluated at 100 values of period (T). PGA_{obs} and PGA_{sim} are the observed and simulated PGA values. The fitness of the inversion is evaluated from the average of Eqs. (7) and (8).

4.2. Resolved asperity and attenuation parameters

We obtained an inversion fitness value of 70% (Eqs. (7) and (8)) for our preferred asperity model. The preferred asperity and attenuation parameters are shown in Table 2.

We found that the ratio of background stress drop to average asperity stress drop is nearly 50%. This value is in agreement with the theoretical asperity model of Das and Kostrov (1986) (circular asperity embedded in a broken crack), namely that the

Table 2

Preferred asperity parameters of the 2000 Tottori earthquake, obtained by optimizing the agreement to observed broadband frequency ground motion

Asperity	Rise time (s)	Rupture velocity (km/s)	Stress drop (bar)	$Q(f)$
1	1.6	2.25	103	$146f^{0.67}$
2	1.6	2.05	196	$146f^{0.67}$
Background	1.7	2.25	71	$146f^{0.67}$

average stress drop of an asperity (with radius r) is increased by the ratio (R/r) over the average stress drop on the surrounding annular crack area (with radius R). This result combined with an empirical ratio of total asperity area to fault rupture area (Somerville et al., 1999), gives a stress drop ratio value of about 0.47.

The effect of Q on high-frequency ground motion is significant in the near-fault region. We found an attenuation of $Q(f)=146f^{0.67}$, for a region within 50 km from the epicenter of the Tottori earthquake. We found an F_s value of nearly 1. This value suggests that the effect of downgoing S-waves is negligible at the borehole depth (100 m).

5. Near-fault ground motion

The velocity waveforms obtained from our preferred asperity model generally agrees very well with the observations (Fig. 7). The acceleration waveforms fit is acceptable as well (Fig. 8). The acceleration response spectra (Fig. 9) also generally agree with the observations. There is a discrepancy for the fault normal component of stations OKYH07 and OKYH14. In the later case, the simulation underestimates the observations for frequencies larger than 5 Hz. We do not have a clear explanation for this discrepancy. We note, however, that station OKYH14 is located exactly on a maximum axis of radiation of SH waves, which is responsible for the very large fault normal component compared with the fault parallel component.

5.1. Ground motion distribution around the fault

In Figs. 10 and 11, we show a comparison between the observed and simulated PGV and PGA

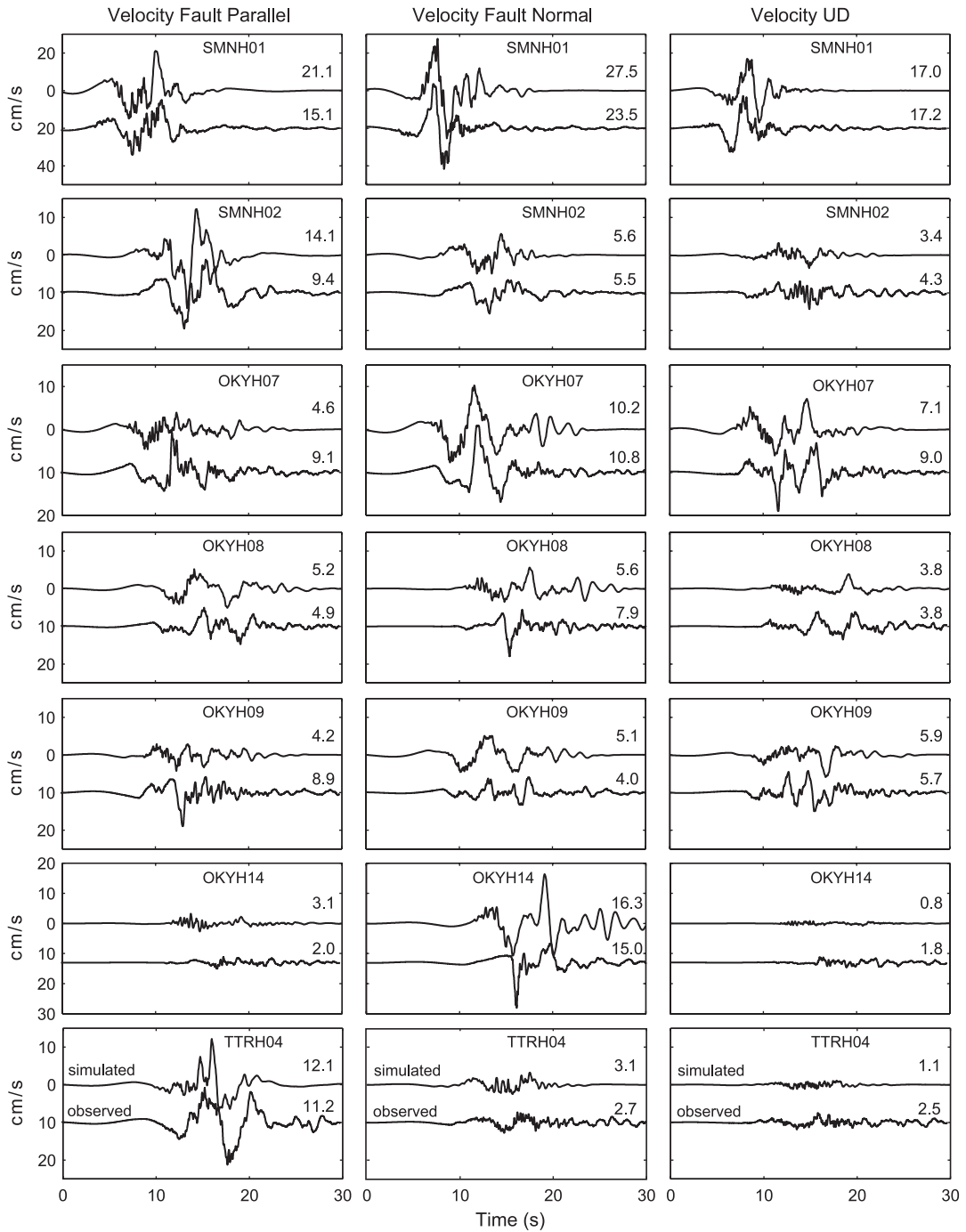


Fig. 7. Comparison between the simulated and observed velocity waveforms (preferred solution). All the data have been bandpassed filtered between 0.1 and 10 Hz.

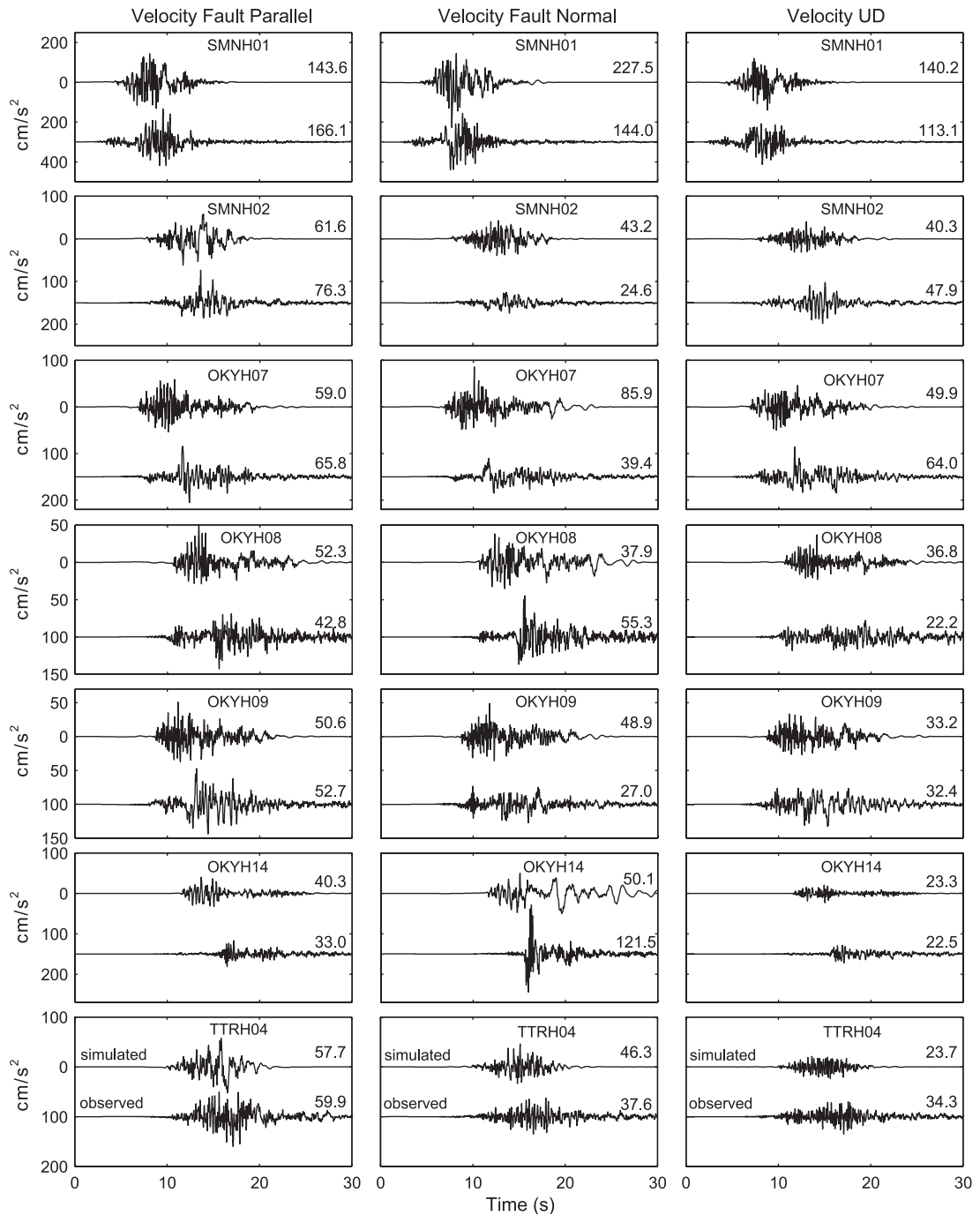


Fig. 8. Comparison between the simulated and observed acceleration waveform (preferred solution). All the data have been bandpassed filtered between 0.1 and 10 Hz.

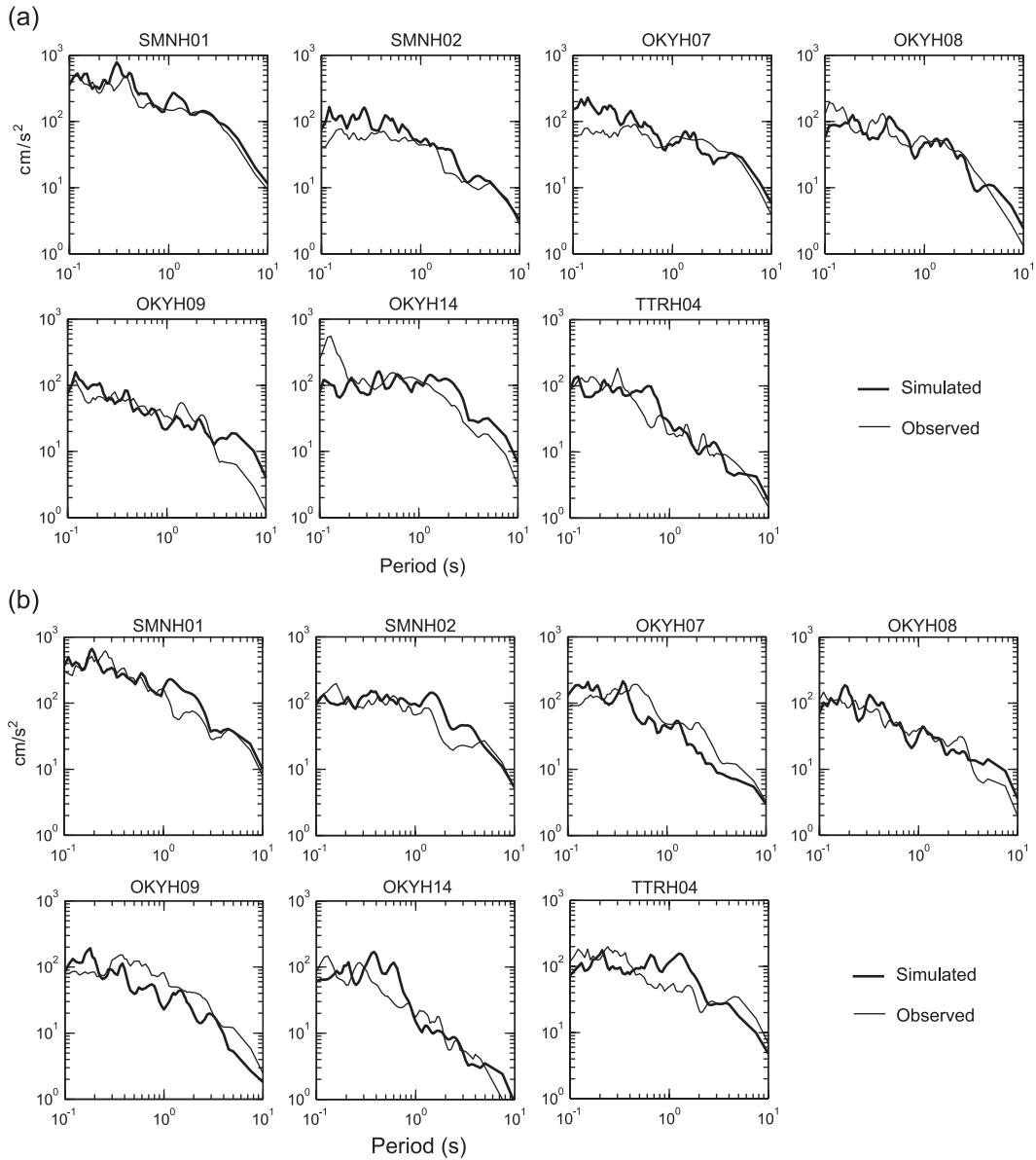


Fig. 9. (a) Comparison between the simulated and observed acceleration response spectra for the Fault Normal component (preferred solution). (b) Same comparison for the Fault Parallel component.

distributions around the fault, plotted by using the KiK-Net stations. We can observe that the agreement is very good in either case. However, the sparse location of the KiK-Net stations do not allow us to retrieve the details of very near-fault ground motion. For that purpose, we performed a forward simulation of the ground motion at a larger number of points

around the fault by using the asperity model obtained previously. We performed the simulation at every 10 km within a region of 90×90 km² around the fault. We estimated the velocity model at every receiver from the nearest KiK-Net station. The simulated PGV distribution around the fault reveals a strong propagation along the Northern and Southern exten-

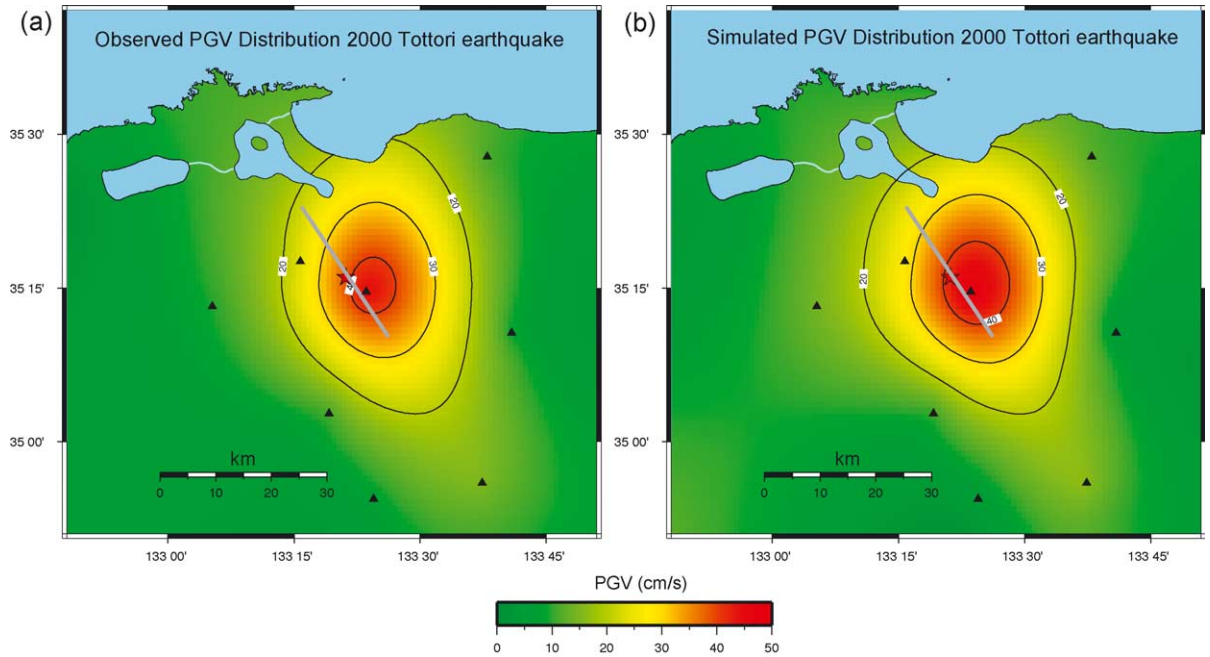


Fig. 10. (a) Simulated Peak Ground Velocity distribution around the fault (only KiK-Net stations). (b) Observed PGV distribution from the KiK-Net borehole stations. Station location are shown by triangles. KiK-Net station locations are shown by small triangles. All the data have been bandpassed filtered between 0.1 and 10 Hz.

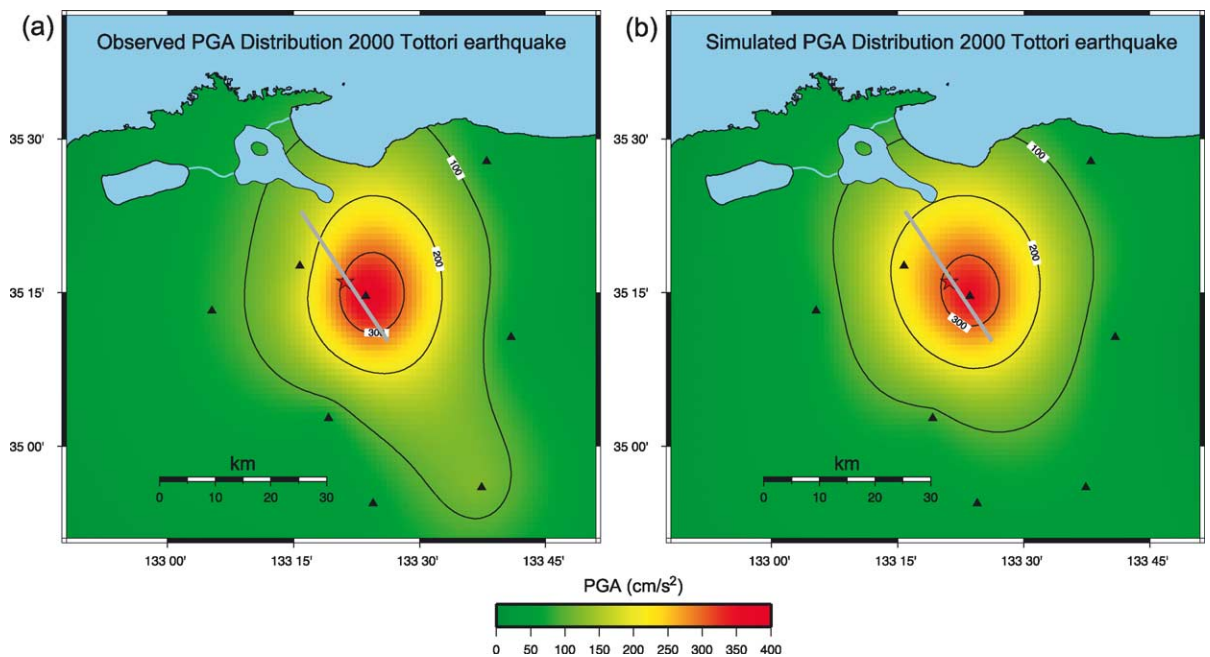


Fig. 11. (a) Simulated Peak Ground Acceleration distribution around the fault (only KiK-Net stations). (b) Observed PGA distribution from the KiK-Net underground stations. Station locations are shown by triangles. KiK-Net station locations are shown by small triangles. All the data have been bandpassed filtered between 0.1 and 10 Hz.

sion of the fault line, in addition to a large ground motion concentration near the epicenter (Fig. 12). Our simulated bedrock PGV values towards the North-West are in agreement with the JMA intensity values from 5 to 6 obtained in the Yumigahama Peninsula (region within the dash line in Fig. 12), from a detailed post-earthquake damage survey in the area (AIJ, 2001).

We can observe that the propagation towards the North-West of the fault is stronger than the South-East propagation. One possible explanation is that for distances close to the fault, asperity 1 (that controls the North-West ground motion) radiates S-waves more efficiently than asperity 2 (that controls the South-East ground motion). This is based on the observation that the S-wave radiation pattern coefficient in the fault plane decreases with increasing depth, which favors the S-wave radiation of asperity 1 compared with the radiation of asperity 2 (Figs. 1 and 6).

The simulated PGA distribution around the fault shows a weaker propagation along the fault line, compared to the PGV distribution (Fig. 13). This may be explained because the PGA values are largely

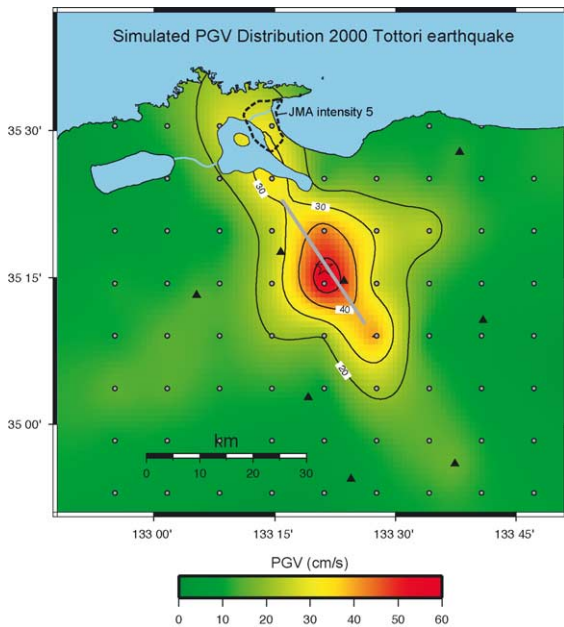


Fig. 12. Simulated PGV distribution for all the simulation points (small circles). KiK-Net stations are also included (small triangles).

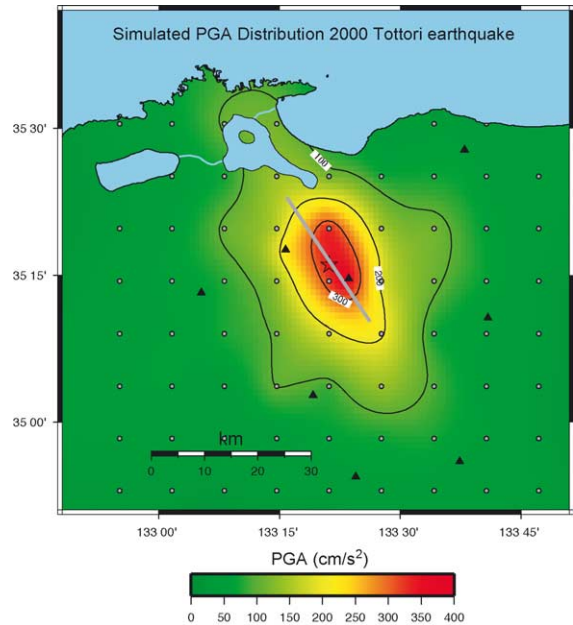


Fig. 13. Simulated PGA distribution for all the simulation points (small circles). KiK-Net stations are also included (small triangles).

controlled by high frequencies, and therefore they have a weaker dependence on the radiation pattern compared with the PGV values.

If we look at the simulated and observed velocity particle motion around the fault (Fig. 14), we see that at epicentral distances larger than half the fault length, the radiation pattern corresponds well to the radiation of S-waves by a double-couple point source. Near the fault, the particle motion is very complex and does not correspond to the radiation from a single point source. The latter would correspond to the fault “near field”.

5.2. Influence of the rupture parameters on the near-fault ground motion

We examined the influence of the asperities and background region rupture velocity and rise time on the ground motion. We performed a forward simulation of ground motion considering two cases: (a) increasing the rupture velocity (V_r) of the asperities and background region by 25%; and (b) reducing the rise time (τ) 25% with respect to the values of the preferred asperity model, hereinafter referred to as “base model”. The remaining asperity parameters were unchanged in either case.

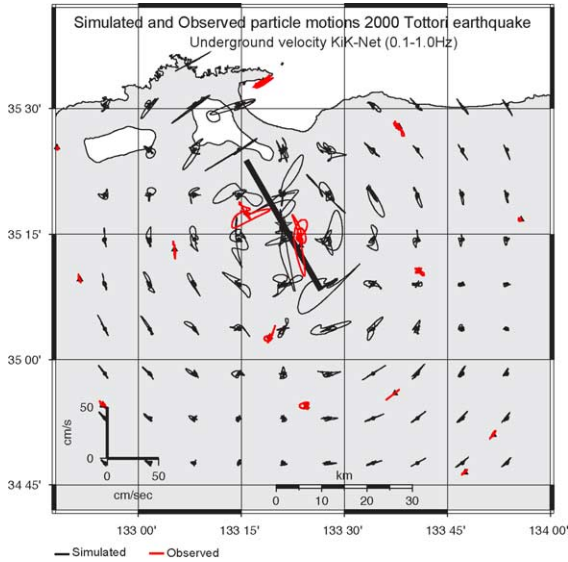


Fig. 14. Velocity particle motion of the observed (red) and simulated (black) stations. The data have been bandpassed filtered between 0.1 and 1.0 Hz. Note that the radiation from a double-couple point source is observed for epicentral distances larger than half the fault length but not for smaller distances.

A 25% increase in the rupture velocity resulted in an increase of up to 50% in the PGV distribution respect to the base model (Fig. 15a). We observed a similar increase in the PGV distribution from a 25% reduction in the rise time (Fig. 15b). From the previous comparisons, we infer that an increase in the rupture velocity produces a similar effect on the ground motion as a reduction in the rise time. Furthermore, fault models with the same V_r/τ ratio for a given seismic moment will produce a very similar PGV distribution around the fault (Fig. 15).

6. Conclusions

We investigated the broadband asperity parameters of the 2000 Tottori earthquake by applying a non-linear inversion scheme combined with a hybrid strong motion simulation method. The good agreement between observed and simulated waveforms and spectra provides a good test for our inversion scheme as well as for the hybrid simulation technique.

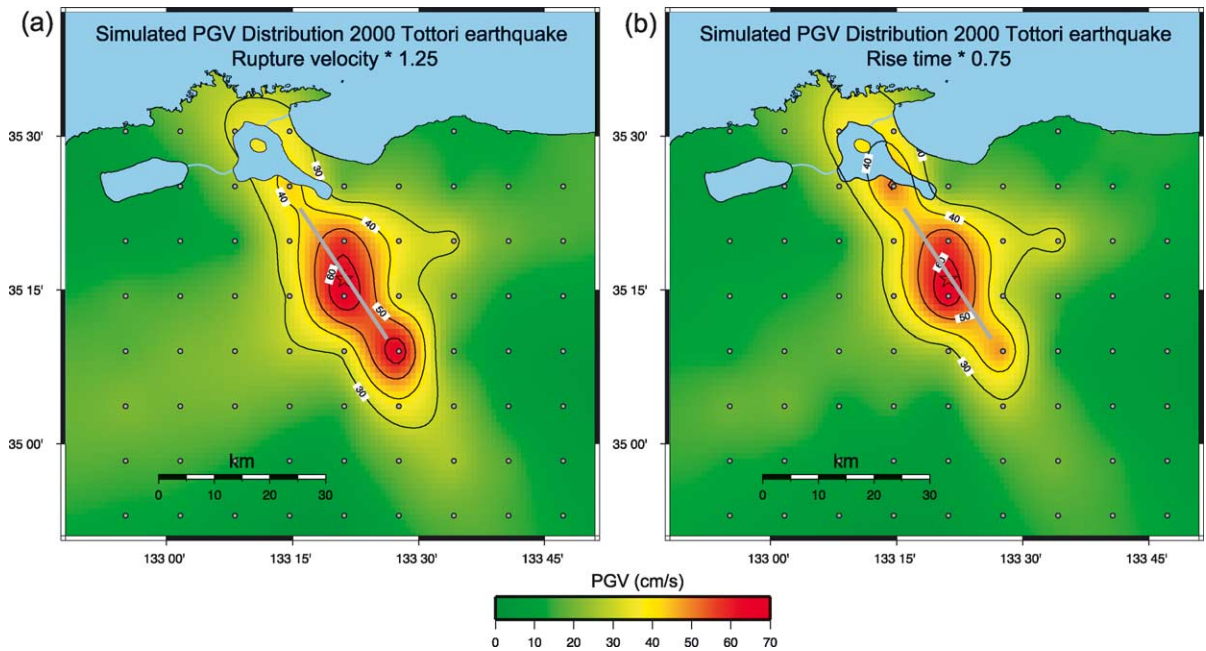


Fig. 15. (a) PGV distribution for a rupture velocity 25% larger than the value of the preferred asperity parameters. (b) PGV distribution for a rise time 25% smaller than the value of the preferred parameters. The simulated PGV values are up to a 50% larger than the PGV from the preferred asperity model for either case.

The ratio of background stress drop to average asperity stress drop from our inversion is nearly 50%, in agreement with the theoretical asperity model of [Das and Kostrov \(1986\)](#), and an empirical ratio of asperities to rupture area ([Somerville et al., 1999](#)). We obtained an attenuation value for the Tottori earthquake near-fault region of $Q(f) = 146f^{0.67}$. Our results suggest that the effect of downgoing S-waves completely disappears at the borehole depth.

The ground motion radiation towards the North-West of the fault is larger than the radiation towards the South-East, despite the smaller seismic moment of asperity 1 compared with asperity 2. A possible explanation is that in the vicinity of the fault, asperity 1 radiates S-waves more efficiently than asperity 2, as inferred from the radiation pattern coefficient distribution within asperities.

The simulated PGA values have a weaker dependence on the radiation pattern compared with the PGV values, in the near-fault region.

The simulated radiation pattern is very complex for epicentral distances within half the fault length but it approaches the radiation of a double-couple point source for larger distances.

The rupture velocity and rise time have significant influence on the PGV distribution around the fault. An increase in rupture velocity produces a similar effect on the ground motion as a reduction in rise time.

Acknowledgments

Comments from K. Kamae, the associate editor K. Shedlock and an anonymous reviewer helped to improve the manuscript. We would like to thank the National Research Institute for Earth Science and Disaster Prevention in Japan (NIED), for providing the KiK-Net data used in this study. Many figures were created using the Generic Mapping Tools (GMT) software ([Wessel and Smith, 1998](#)).

References

- AIJ, T., 2001. Report on the damage investigation of the 2000 Western Tottori prefecture earthquake and the 2001 Geiyo earthquake. Architectural Institute of Japan, AIJ, pp. 11–14.
- Akazawa, T., Kagawa, T., 2000. A study on frequency dependent radiation pattern (part2). Fall Meeting of the Seismological Society of Japan.
- Aki, K., Richards, P., 2002. *Quantitative Seismology*. (2nd ed.) University Science Books.
- Boore, D.M., 1983. Stochastic simulation of high frequency ground motions based on seismological models of the radiation spectra. *Bull. Seismol. Soc. Am.* 73, 1865–1894.
- Boore, D.M., Boatwright, J., 1984. Average body-wave radiation coefficients. *Bull. Seismol. Soc. Am.* 74 (5), 1615–1621.
- Bouchon, M., 1981. A simple method to calculate Green's functions for elastic layered media. *Bull. Seismol. Soc. Am.* 71 (4), 959–971.
- Brune, J.N., 1970. Tectonic stress and the spectra of seismic shear waves from earthquakes. *J. Geophys. Res.* 75, 4997–5009.
- Das, S., Kostrov, B.V., 1986. Fracture of a single asperity on a finite fault: a model for weak earthquakes? *Earthquake Source Mechanics*. AGU, pp. 91–96.
- DPRI, 2000. Crustal Velocity Structure of the Tottori Region (Personal Communication). Disaster Prevention Research Institute (DPRI), Kyoto University.
- Houck, C.R., Joines, J.A., Kay, M.G., 1995. A genetic algorithm for function optimization: a Matlab implementation. Technical Report NCSU-IETR-95-09, North Carolina State University.
- Irikura, K., 1986. Prediction of strong acceleration motion using empirical Green's function. 7th Japan Earthq. Eng. Symp., pp. 151–156.
- Iwata, T., Sekiguchi, H., Matsumoto, Y., Miyake, H., Irikura, K., 2000. Source process of the 2000 Western Tottori Prefecture earthquake and near-source strong ground motions. Fall Meeting of the Seismological Society of Japan.
- Kamae, K., Irikura, K., Fukuchi, Y., 1990. A study of ground motion prediction procedure using empirical green's function. 8th Japan Earthquake Engineering Symp., pp. 223–228.
- Kamae, K., Irikura, K., Pitarka, A., 1998. A technique for simulating strong ground motion using hybrid Green's function. *Bull. Seismol. Soc. Am.* 88 (2), 357–367.
- Liu, H.L., Helmberger, D.V., 1985. The 23:19 aftershock of the 15 October 1979 Imperial valley earthquake: more evidence for an asperity. *Bull. Seismol. Soc. Am.* 75, 689–708.
- Pitarka, A., Irikura, K., Iwata, T., Sekiguchi, H., 1998. Three-dimensional simulation of the near-fault ground motion for the 1995 Hyogo-ken Nanbu (Kobe), Japan, Earthquake. *Bull. Seismol. Soc. Am.* 88 (2), 428–440.
- Pitarka, A., Somerville, P., Fukushima, Y., Uetake, T., Irikura, K., 2000. Simulation of near-fault strong-ground motion using hybrid green's function. *Bull. Seismol. Soc. Am.* 90 (3), 566–586.
- Pulido, N., 2002. Radiation pattern model for high frequency strong ground motion simulation. Japan Earth and Planetary Science Joint Meeting, Abstracts, pp. S018-P012.
- Satoh, T., 2002a. Empirical frequency-dependent radiation pattern of the 1998 Miyagiken–Nanbu earthquake in Japan. *Bull. Seismol. Soc. Am.* 92 (3), 1032–1039.
- Satoh, T., 2002b. Radiation pattern and f_{\max} of the Tottori-ken Seibu earthquake and the aftershocks inferred from KiK-Net strong

- motion records. *J. Struct. Constr. Eng.*, AIJ 556, 25–34. in Japanese.
- Somerville, P., Irikura, K., Graves, R., Sawada, S., Wald, D., Abrahamson, N., Iwasaki, Y., Kagawa, T., Smith, N., Kowada, A., 1999. Characterizing crustal earthquake slip models for the prediction of strong ground motion. *Seismol. Res. Lett.* 70 (1), 59–80.
- Takenaka, H., Mamada, Y., Futamura, H., 2003. Near-source effect on radiation pattern of high-frequency S waves: strong SHSV mixing observed from aftershocks of the 1997 Northwestern Kagoshima, Japan, earthquakes. *Phys. Earth Planet. Inter.* 137, 31–43.
- Wessel, P., Smith, W.H.F., 1998. New improved version of generic mapping tools released. *EOS, Trans. Amer. Geophys. Union* 79 (47), 579.